Applied Catalysis B: Environmental 84 (2008) 457–467

Contents lists available at ScienceDirect

Applied Catalysis B: Environmental

journal homepage: www.elsevier.com/locate/apcatb

Effect of strontium and cerium doping on the structural characteristics and catalytic activity for C_3H_6 combustion of perovskite $LaCrO_3$ prepared by sol–gel

K. Rida [a], A. Benabbas [a], F. Bouremmad [a], M.A. Peña [b], E. Sastre [b], A. Martínez-Arias [b,*]

[a] Laboratoire d'Etudes sur les Interactions Materiaux-Environnements, Université de Jijel, Algeria
[b] Instituto de Catálisis y Petroleoquímica, CSIC, C/Marie Curie 2, Campus de Cantoblanco, 28049 Madrid, Spain

ARTICLE INFO

Article history:
Received 13 March 2008
Received in revised form 22 April 2008
Accepted 29 April 2008
Available online 14 May 2008

Keywords:
Perovskite
$LaCrO_3$
Sr and Ce doping
Sol–gel
C_3H_6 oxidation
SOFC

ABSTRACT

Two series of Sr- or Ce-doped $La_{1-x}M_xCrO_3$ (x = 0.0, 0.1, 0.2 and 0.3) catalysts were prepared by thermal decomposition of amorphous citrate precursors followed by annealing at 800 °C in air atmosphere. The effect of Ce and Sr on the morphological/structural properties of $LaCrO_3$ was investigated by means of thermogravimetric/differential thermal analysis (TG/DTA) of the precursors decomposition under air, X-ray diffraction (XRD), electron paramagnetic resonance (EPR), transmission electron microscopy–X-ray energy dispersive spectroscopy (TEM–XEDS), S_{BET} determination, scanning electron microscopy (SEM) and X-ray photoelectron spectroscopy (XPS) techniques. The characterization results are employed to explain catalytic activity results for C_3H_6 combustion. It is shown that the lanthanum chromite perovskite structure is obtained upon thermal treatment of the sol–gel derived precursors at $T >$ ca. 800 °C. The presence of the dopant generally induces the formation of segregated oxide phases in the samples calcined at 800 °C although some introduction of the Sr in the perovskite structure is inferred from EPR measurements. The oxidation activity becomes maximised upon formation of such doped perovskite structure.

1. Introduction

The lanthanum chromite perovskite $LaCrO_3$ and compositions derived from it by substituting lanthanum by other metal cations ($La_{1-x}M_xCrO_3$) present a high mechanical and chemical stability while displaying high melting points, large electrical conductivity and a relatively high catalytic oxidation activity [1–6]. Such properties make them most interesting for their application to various environmental issues as components of solid oxide fuel cells, in which they can be employed as interconnect or electrode materials, as well as for catalytic applications requiring highly refractory materials (high temperature treatment of exhaust gases, furnace electrodes, etc.) [7–13].

The ideal ABO_3 perovskite structure belongs to the cubic group $Pm3m$. Upon changing the size of the cation at the A position with respect to the ideal situation, the BO_6 octahedra become rotated about the cubic crystallographic axis, which affects the structural stress as a result of changes in the B–O–B bond angle; in turn, changes in the coordination number of the A cations, with associated generation of structural defects, can also occur [1,14]. Structural defects can also arise upon partial substitution of the cation in the A position by other metal cations; such defects (typically oxygen vacancies) can result beneficial from a catalytic point of view since their presence could favour reactants chemisorption or other relevant catalytic steps (oxygen transport, electron transfer processes, etc.) [1,5,13,15–20].

Perovskite-type oxides are usually synthesized by a variety of methods including ceramic solid state reaction, co-precipitation, spray drying, freeze-drying and sol–gel (in particular, employing amorphous citrate complexes) ones [1]. Among them, high surface area along with high chemical homogeneity at structural level can in principle be achieved by the freeze-drying and sol–gel amorphous citrate methods [17]. In this context, the present work aims to explore the catalytic properties for the combustion of propene (chosen as representative of hydrocarbon exhaust gases) of two series of, respectively, Sr- or Ce-doped $LaCrO_3$ perovskite materials prepared by a sol–gel method; it may be noted that results on the catalytic properties of this specific type of perovskites appear relatively scarce despite their significant technological potential. For the mentioned purpose, the evolution of the sol–gel derived catalyst precursor has been investigated by TGA–DTA in order to select optimum preparation parameters for

* Corresponding author. Tel.: +34 915 85 49 40; fax: +34 915 85 47 60.
E-mail address: amartinez@icp.csic.es (A. Martínez-Arias).

0926-3373/$ – see front matter © 2008 Elsevier B.V. All rights reserved.
doi:10.1016/j.apcatb.2008.04.031

the various catalysts. The structural and other physicochemical characteristics of the obtained materials have been explored by XRD, S_{BET} measurements, electron microscopies, EPR and XPS in order to rationalize their catalytic behaviour.

2. Experimental

2.1. Preparation

$La_{1-x}A_xCrO_3$ oxides (A = Sr, Ce), with x = 0, 0.1, 0.2 and 0.3, were prepared by a sol–gel (Pechini) method employing citric acid as complexing agent. The required amounts of the precursor salts ($La(NO_3)\cdot 6H_2O$, $Sr(NO_3)_2$, $Ce(NO_3)\cdot 6H_2O$ or $Cr(NO_3)_3\cdot 9H_2O$) along with citric acid were dissolved in water at an equivalent ratio of 1:1 (metal cations:citric acid). The resulting solutions were heated to 80 °C to form a viscous gel which finally yield a solid precursor upon slow solvent evaporation at that temperature for several hours; this was then treated at 400 °C for 1 h and after thorough grinding of the resulting powder in a mortar, it was finally calcined (in accordance to TG/DTA analysis, *vide infra*) under air at 800 °C for 5 h in order to achieve the corresponding perovskite structure in the samples (*vide infra*). A CeO_2 reference catalyst was prepared by calcining under air at 800 °C for 2 h a commercial ceria sample provided by Rhodia.

2.2. Characterization

Thermogravimetric analysis (TGA) and differential thermal analysis (DTA) of the decomposition of the precursor solid obtained after solvent evaporation at 80 °C were performed on PerkinElmer TGA7 and PerkinElmer DTA7 devices, respectively, in a ramp from 25 to 900 °C at a heating rate of 10 °C min^{-1}, under air flow of ~60 ml min^{-1}.

Powder X-ray diffraction (XRD) patterns were recorded in the 10–80° 2θ range in the scan mode (0.02° step size, 2 s counting time) using a D8-Advance Bruker-AXS powder diffractometer employing Cu Kα radiation. The unit cell parameters were obtained by refining the peak positions of the XRD pattern with a least squares method and employing the CELREF program (unit cell refinement software). For the determination of peak positions, the peak profiles were fitted with the WINPLOTR program. The crystalline particle sizes were calculated from analyses of Williamson–Hall plots from which possible contributions of microstrain to the peaks width were also estimated [21,22]. The specific surface area of the samples was determined by the BET method applied to nitrogen adsorption isotherms taken at −196 °C using a Micrometrics apparatus model ASAP-2000. Prior to data recording, the samples were degassed for 2 h at 140 °C.

The general morphology of the ground samples was analysed by scanning electron microscopy (SEM) using a Philips XL30 apparatus.

X-ray photoelectron spectroscopy (XPS) studies were performed with a VG Escalab 200R spectrometer employing an Mg Kα (1253.6 eV) X-ray source. The sample was first placed in a copper holder mounted on a sample-rod in the pre-treatment chamber of the spectrometer and then outgassed at room temperature for 1 h before being transferred to the analysis chamber. The desired region of the spectrum was then scanned a number of times in order to obtain a good signal-to-noise ratio. The binding energies (BE) were referenced to the spurious C 1s peak (284.6 eV) used as an internal standard to take into account charging effects. The areas of the peaks were computed by fitting the experimental spectra to Gaussian/Lorenztian curves after removal of the background (Shirley function). Surface atom ratios were calculated from peak area ratios normalized by the appropriate atomic sensitivity factors [23].

The electron paramagnetic resonance (EPR) measurements were done with a Bruker ER200D spectrometer operating in the X-band and calibrated with a DPPH standard. The spectra were typically performed at −196 °C (some of them also at room temperature, ca. 25 °C) using a conventional spectroscopic quartz tube cell (4 mm o.d.) employed for studies of solid samples. Aliquots of the sample (between 20 and 30 mg) were thoroughly treated under high vacuum conditions at room temperature prior to measurement.

Transmission electron microscopy–X-ray energy dispersive spectroscopy (TEM–XEDS) examination of the samples was done with a high resolution electron microscope JEOL JEM 2100 F UHR. Specimens were prepared by depositing particles of the samples to be investigated from ethanol dispersion onto a copper grid supporting a perforated carbon film.

2.3. Catalytic activity tests

The catalysts were tested for the C_3H_6 oxidation reaction at atmospheric pressure. Powder catalyst sample (750 mg, sieved to 0.125–0.250 mm particles) was mixed homogeneously with SiC (total volume of 2 ml) in order to reduce the volumetric heat release. The mixture was loaded in a Pyrex reactor tube (5 mm i.d). Prior to catalytic tests, the catalysts were treated under synthetic air stream at 450 °C followed by purging in a N_2 flow. The flow rate employed for the tests was of 40,000 ml h^{-1} g^{-1} and the feed composition consisted in 0.3% C_3H_6 and 5.4% O_2 (vol.%; N_2 balance). Analysis of the feed and outlet gas streams was done by gas infrared spectroscopy (PerkinElmer FTIR spectrometer model 1725X, coupled to a multiple reflection transmission cell – Infrared Analysis Inc. "long path gas minicell", 2.4 m path length, *ca.* 130 cm^3 internal volume–) while a paramagnetic analyser (Servomex 540 A) was used to analyse the O_2 concentration.

3. Results and discussion

3.1. TG/DTA analysis of the precursors

With the aim of exploring the evolution of the sol–gel derived samples during the course of the calcination treatment and also in order to select optimum synthesis conditions under which the $La_{1-x}M_xCrO_3$ perovskite structure could become formed, while simultaneously getting information on the lowest possible calcination temperature in order to maintain the highest possible specific surface in them, the precursor powders obtained at 80 °C (see Section 2) of representative samples within each series were examined by TG/DTA (Fig. 1). For the $LaCrO_3$ precursor, a relatively small weight loss (of ca. 2%) is observed between 20 and ca. 450 °C (with an inflection point at ca. 110 °C), in correlation with a broad endothermic peak. This most likely corresponds mainly to desorption of chemisorbed or hydration water that may remain in the precursor, in accordance with previous works [24–26]. A second apparent weight loss is produced between ca. 450 and 600 °C in coincidence with observation of a relatively large exothermic peak centred at 515 °C. After the initial loss of water from the precursor, the decomposition of the citrate by decarboxylation is expected. However, the experimental weight loss observed in this range (ca. 8%) appears too low in comparison with the value expected if the metals were fully complexed by citrate species (higher than 50%) in the initial precursor. Besides, the temperature of the exothermic peak (515 °C) is higher than that found for pure citrates [26,27]. It could be concluded that this second decomposition step does not correspond to the citrate decomposition process, and the explanation can be found by analysing the processes that could take place during the drying

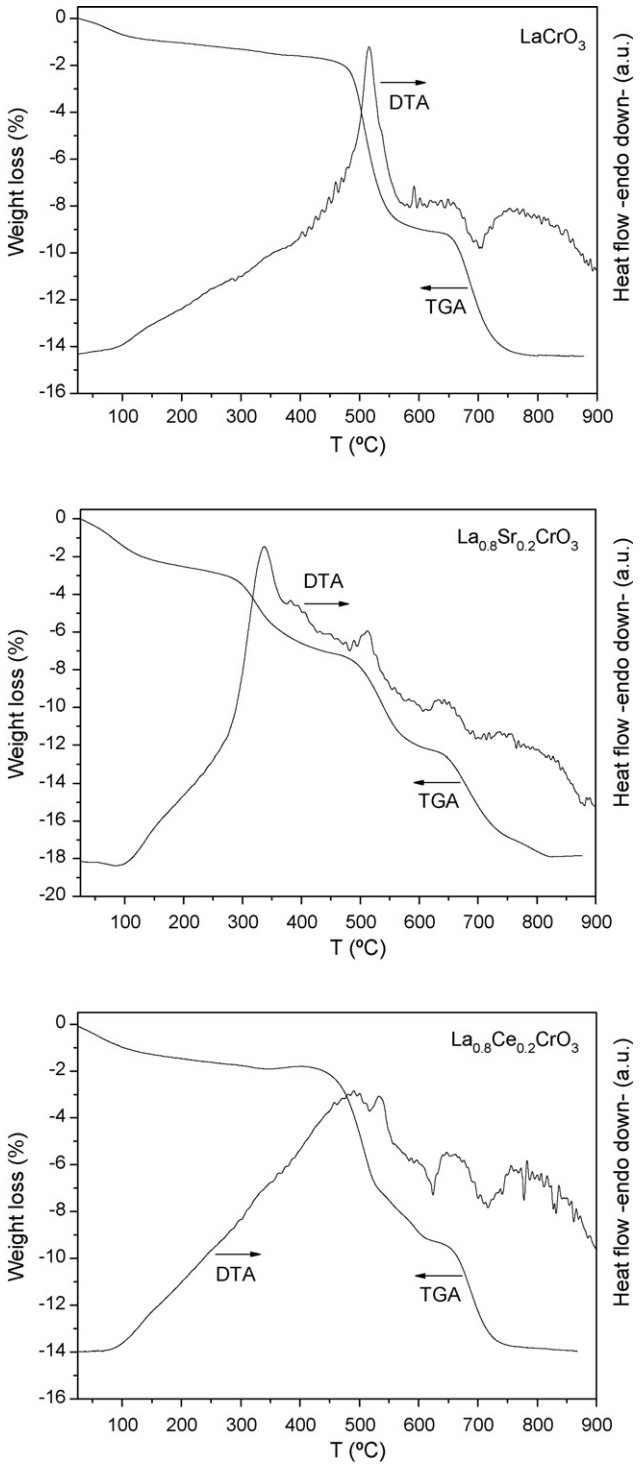

Fig. 1. TG/DTA curves for the powder precursors of the indicated samples (see text).

process at 80 °C of the citrate precursor. In this sense, when nitrates are used as metal precursors, nitric acid can be formed in the solution during gelation of the citrates. After heating up to dryness, water and most of the nitric acid is removed, but a substantial amount of nitric anion can remain adsorbed on the citrate gel. During the final drying of the precursor at nominally 80 °C, and depending on the drying conditions and nature of the metals, these nitrate species can act as a strong oxidants and decompose the citrates during the treatment in the drying oven; note that such exothermic process can produce a remarkable rise of the bulk temperature of the precursor which would favour this citrate decomposition process. As a consequence, the resulting precursor is not actually a citrate, but rather an intermediate product from its decomposition, probably carbonate or oxycarbonate and, to some extent, the metal oxides [24,28,29]. This hypothesis has been supported by IR results in a former contribution in which further details of the decomposition process were reported [29]. Accordingly, the second weight loss centred at 515 °C (ca. 8%) can be ascribed to the decomposition of the remaining carbonates and oxycarbonates to produce an oxide phase. A final appreciable weight loss (ca. 5%) is observed between ca. 630 and 800 °C in correlation with an endothermic peak centred at ca. 700 °C. This process most likely corresponds mainly to an oxygen loss from reduction of an intermediate lanthanum chromate phase resulting in final generation of the lanthanum chromite perovskite [24,25,30], in agreement with previous results [29].

In the case of the doped samples, even though strong similarities are encountered in comparison with the TG/DTA profiles of $LaCrO_3$, some extra features are apparent. For the Sr-doped sample, a first relatively large exothermic peak, accompanied by a ca. 4% weight loss, appears at ca. 300 °C. This is in agreement with previous results obtained on samples of this type and suggests that the presence of strontium can facilitate the combustion of the carbonates or oxycarbonates resulting from citrate decomposition in this sample [24]. For the Ce-doped sample, an extra relatively small endothermic peak appears at ca. 630 °C while the weight loss profile in the 500–600 °C zone (apparently associated to exothermic contributions) appears somewhat more complex than that observed for the undoped sample. These suggest that the presence of cerium can somewhat retard decomposition of the carbonates or oxycarbonates resulting from citrate decomposition (related to the exothermic weight loss), which is in agreement with the basic character of oxygen associated to cerium cations or ceria itself (known to form a segregated phase in this sample in accordance with XRD results presented below) [31], while favouring also crystalline transformations not associated to weight changes (peak at ca. 630 °C), known to take place in this type of complex doped chromate–chromite materials [24].

On the basis of this TG/DTA analyses, and in agreement also with previous work [29], 800 °C has been chosen (as described in Section 2) as the most adequate calcination temperature to obtain by this method optimum balance between achievement of the chromite perovskite structure (in agreement also with XRD experiments discussed next) and maintenance of the largest possible surface area. It must be noted that this latter can appreciably decrease as a consequence of thermal sintering if higher calcination temperature is applied [29].

3.2. Structural and morphological characteristics of the $La_{1-x}M_xCrO_3$ samples

The X-ray diffraction patterns of the Sr- and Ce-doped samples calcined at 800 °C are shown in Figs. 2 and 4, respectively. The main peaks of the XRD pattern for the undoped sample ($x = 0.0$) and the lattice parameters extracted from them (Table 1) agree well with those of the orthorhombic (*Pnma* space group) perovskite-type structure of the lanthanum chromite [32,33]; the presence of this structure as a single phase for the undoped La–Cr oxide sample calcined at 800 °C is in agreement with TG/DTA analysis (Fig. 1). As observed in the diffractograms for the two series of samples, such phase is the major one in any of the samples. Analysis of the lattice parameters for this perovskite phase as a function of the degree of doping shows no important difference, except for $x = 0.3$ in the

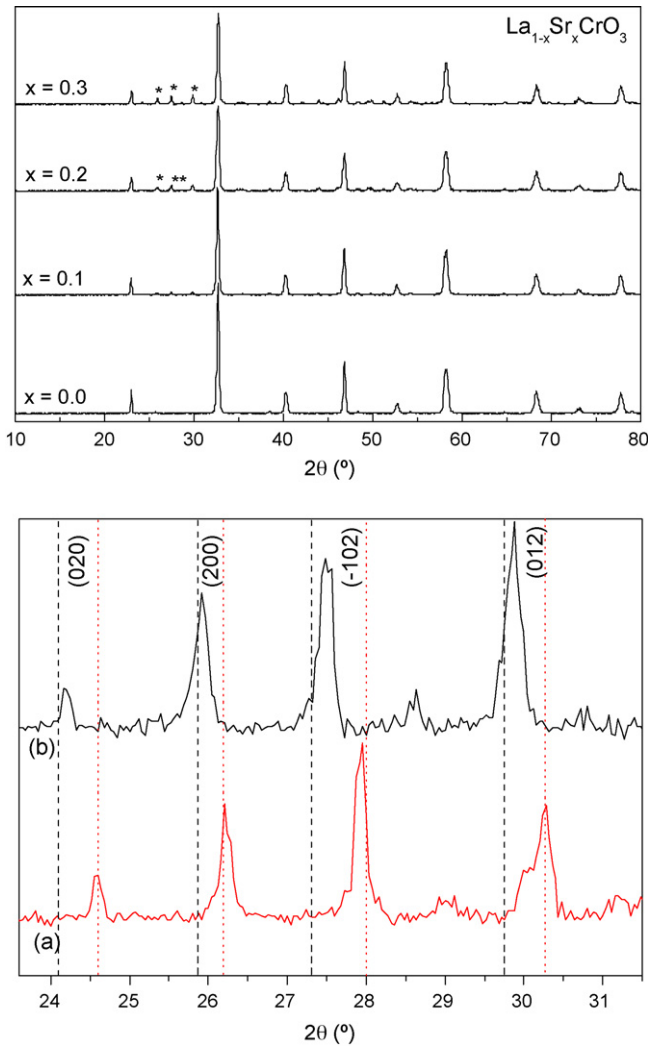

Fig. 2. X-ray diffractograms for the samples of the $La_{1-x}Sr_xCrO_3$ series (top). Asterisk marks indicate peaks attributed to segregated $SrCrO_4$ (see text). The bottom graphic compares a detail of the diffractogram of the $La_{0.7}Sr_{0.3}CrO_3$ sample (b) with that of a similar Sr-free sample prepared by sol–gel and calcined at 600 °C (a); see text for details.

Ce-doped series. Thus, only a slight unit cell volume decrease upon increasing Sr content is detected for the Sr-doped series. This contrasts with recent results obtained for similar samples prepared by solid state reaction at 1200 °C, for which a noticeable lattice contraction (of ca. 0.5% in volume) was detected for $x = 0.1$ doping level, in agreement with achievement of an appreciable level of substitution of La by Sr into the A-site of the perovskite structure and formation of the corresponding solid solution at such doping level [32,34], also consistent with the maximum Sr solubility level expected from thermodynamic calculations [35]. Therefore, the results suggest that strontium introduction into the orthorhombic lanthanum chromite lattice can be more limited for samples prepared by the sol–gel method followed by calcination at 800 °C than for samples prepared by solid state reaction. In this respect, analysis by means of Williamson–Hall of the microstrain evolution as a function of the doping level does not appear conclusive enough, given the correlation found between such parameter and particle size. This suggests that such factor does not reflect to an appreciable extent the possible changes in the amount of defects that could be produced upon doping [34,36]. Nevertheless, EPR investigation of the Sr-doped samples, Fig. 3, shows the presence of a more or less symmetric signal centred at $g = 1.95$ and with ca. 180 G linewidth onto which there appear overlapped other narrow features in the spectra taken at −196 °C. This contrasts with the spectrum of the undoped sample for which only a very weak narrow feature at $g \approx 2.00$, most likely due to carbonaceous impurities, is detected in the spectrum recorded at −196 °C. The signal at $g = 1.95$ detected in the doped samples can be attributed to structural Cr^{3+} cations in distorted "CrO_6" octahedra, while the narrow features most likely originate from more or less isolated Cr^{3+} cations, which could be located at the surface of the sample [34,37]. The lack of observation of Cr^{3+} signals in the spectrum of the undoped sample registered at −196 °C is consistent with antiferromagnetic coupling of the Cr^{3+} cations in the perovskite structure. In this sense, the spectrum recorded for this sample at 25 °C do in fact show a broad signal (Fig. 3 inset), in agreement with an antiferromagnetic to paramagnetic transition proposed to take place between −196 and 25 °C for $LaCrO_3$ [34]. Observation of the Cr^{3+} signals for the doped samples suggests some Sr introduction into the perovskite structure of the chromite, likely higher for the $x = 0.2$ material considering the higher EPR intensity detected for it (Fig. 3), considering that such Sr presence has been proposed to lower significantly the magnetic transition temperature [34].

In any case, a relatively poor Sr solubility into the chromite structure of the samples prepared by the sol–gel method, in contrast to those obtained by solid state reaction [18], is inferred not only by the relatively small lattice contraction (Table 1) but also from the presence in the diffractograms of the Sr-doped samples of extra peaks (marked with an asterisk in Fig. 2) whose intensity increase with the doping degree. They are similar to those expected for a monazite chromate phase (monoclinic; $P2_1/n$ space group [30,38]). Careful analysis of the zone where peaks for this specific phase are most intense, comparing those detected for a Sr-free sample, which exhibits the presence of the monazite $LaCrO_4$ phase (in accordance with those detected for the pure compound [30]), with those expected for a pure monazite $SrCrO_4$ sample [38], reveals that this latter must be the phase which is formed upon Sr

Table 1
Structural and textural parameters of the $La_{1-x}M_xCrO_3$ (M = Sr, Ce) samples calcined at 800 °C

Sample	Lattice parameters (Å)[a]			Unit cell volume (Å^3)[a]	Crystal size (nm)[a]	Microstrain ($\Delta d/d$)[a]	Average particle aggregates size (μm)[b]	S_{BET} ($m^2\ g^{-1}$)
	a	*b*	*c*					
$LaCrO_3$	5.481	5.493	7.756	233.50	125	0.0013	0.588	3.5
$La_{0.9}Sr_{0.1}CrO_3$	5.481	5.496	7.752	233.54	83	0.0015	0.613	3.2
$La_{0.8}Sr_{0.2}CrO_3$	5.485	5.486	7.756	233.36	58	0.0023	0.725	2.5
$La_{0.7}Sr_{0.3}CrO_3$	5.483	5.489	7.749	233.21	84	0.0015	0.732	1.1
$La_{0.9}Ce_{0.1}CrO_3$	5.482	5.488	7.755	233.35	106	0.0013	0.471	4.0
$La_{0.8}Ce_{0.2}CrO_3$	5.488	5.486	7.754	233.44	54	0.0022	0.176	6.5
$La_{0.7}Ce_{0.3}CrO_3$	5.469	5.485	7.718	231.51	22	0.0033	0.118	7.7

[a] For the lanthanum chromite perovskite phase, from analysis of XRD data. Crystal size and microstrain values obtained from analyses of Williamson-Hall plots.
[b] From SEM images.

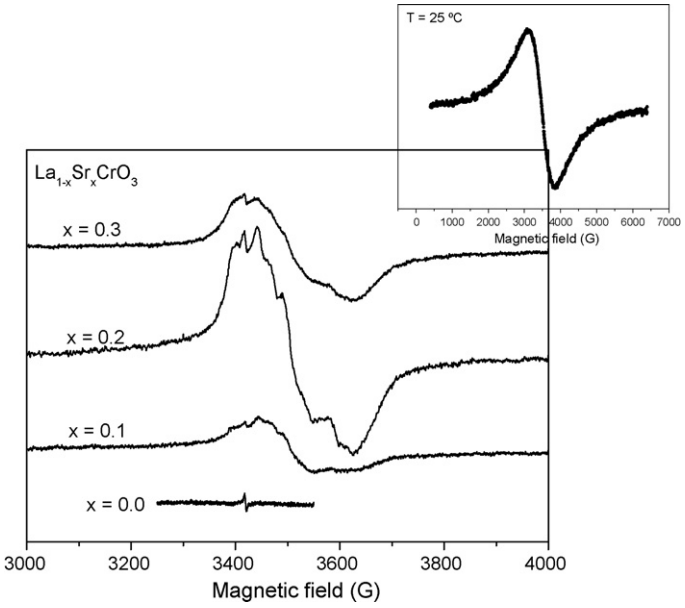

Fig. 3. EPR spectra at −196 °C for the samples of the $La_{1-x}Sr_xCrO_3$ series. The inset at the top right displays the spectrum of the undoped $LaCrO_3$ sample recorded at 25 °C.

doping (note that exact match between peaks can critically depend on small changes in the specific stoichiometry of the corresponding phase in each case).

In the case of the Ce-doped samples (Fig. 4), the absence of significant changes in the lattice parameters values for the lanthanum chromite perovskite phase up to $x = 0.2$ doping level suggests no significant cerium incorporation into the lattice, in agreement with the difficulties observed for such incorporation in materials of this type [39,40]. The higher difficulties for cerium insertion (in comparison to strontium), at least under the oxidative preparation conditions employed, into the lanthanum chromite perovskite structure can be related to differences in the respective ionic radius (1.44, 1.36 and 1.14 for Sr^{2+}, La^{3+} and Ce^{4+}, respectively) which could make cerium doping only favourable in the presence of an oxygen deficient chromite lattice [40]. In accordance with this, the presence of segregated fluorite CeO_2 phase, as well as peaks related to the presence of Cr_2O_3, is detected for any doping level (Fig. 4). This reveals, as in the case of the Sr-doped samples, that segregation of the dopant is generally accompanied by that of chromium and leaves the characteristics of the chromite lattice practically unchanged. An exception to such behaviour is however detected for the sample doped with cerium at $x = 0.3$ for which, despite the increase of both CeO_2 and Cr_2O_3 segregated phases, an appreciable change in the lattice parameters of the orthorhombic chromite phase is detected (Fig. 3 and Table 1). However, the larger amount of segregated CeO_2 and Cr_2O_3 phases detected for this sample suggests that rather than cerium incorporation to the chromite lattice, the generation of other defects (like cationic vacancies or A-site deficient perovskite [16]) into the lanthanum chromite has taken place; further experiments would be however required to confirm this hypothesis. EPR spectra for samples of this series (shown in Fig. 5) display a symmetric signal centred at $g = 1.96$ and with ca. 30 G linewidth, which most likely originates from Cr^{5+} species, typically observed to form in the small Cr_2O_3 particles [41].

TEM–XEDS analysis confirms the presence of segregated phases in the doped samples (Fig. 6). Thus, while images for the undoped $LaCrO_3$ specimen display the presence of aggregates of particles with irregular shape and in which the multiple XEDS analyses performed are consistent with values expected for the corresponding lanthanum chromite composition and showing relatively good compositional homogeneity, the images taken for the $La_{0.8}Sr_{0.2}CrO_3$ and $La_{0.8}Ce_{0.2}CrO_3$ specimens display the presence of separate particles. In this sense, XEDS analysis performed in different positions over the pictures taken for $La_{0.8}Ce_{0.2}CrO_3$ allow to identify the presence of small segregated CeO_2 particles which apparently form on top of relatively large particles basically composed essentially by lanthanum chromite. None of the multiple XEDS spectra taken could however identify the presence of separated chromium oxide particles in this sample, suggesting that the corresponding crystals could be relatively more disperse in the sample. In turn, segregated strontium chromite in $La_{0.8}Sr_{0.2}CrO_3$ appears to form relatively big particles which appear well separated and more or less independent from lanthanum chromite particles.

To summarize structural properties, the lanthanum chromite perovskite structure appears at all examined doping levels for the samples calcined at 800 °C. However, the results for the Sr-doped samples are consistent with the formation of a segregated strontium chromate phase in an amount which increases upon increasing the doping level and apparently forming relatively large particles separated from $LaCrO_3$ (or slightly Sr-doped $LaCrO_3$, in accordance with EPR results) particles. Introduction of a small

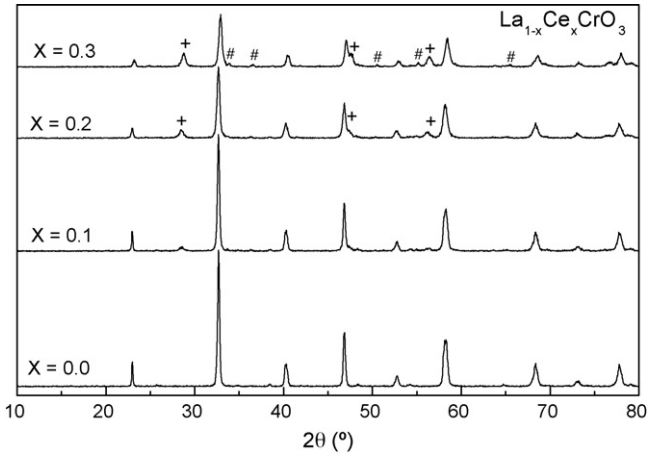

Fig. 4. X-ray diffractograms for the samples of the $La_{1-x}Ce_xCrO_3$ series. + and # marks indicate the presence of segregated CeO_2 and Cr_2O_3 phases, respectively (see text for details).

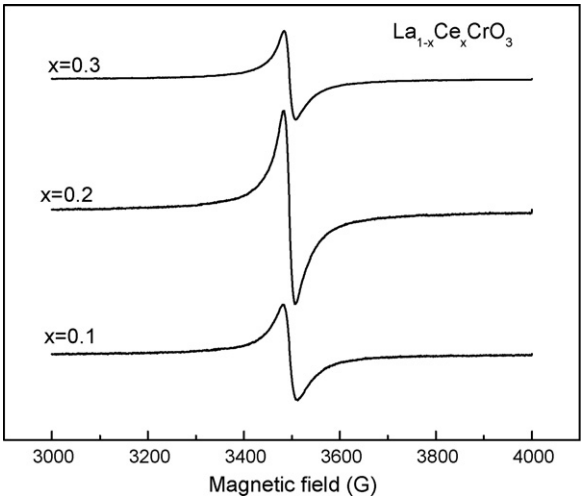

Fig. 5. EPR spectra at −196 °C for the samples of the $La_{1-x}Ce_xCrO_3$ series.

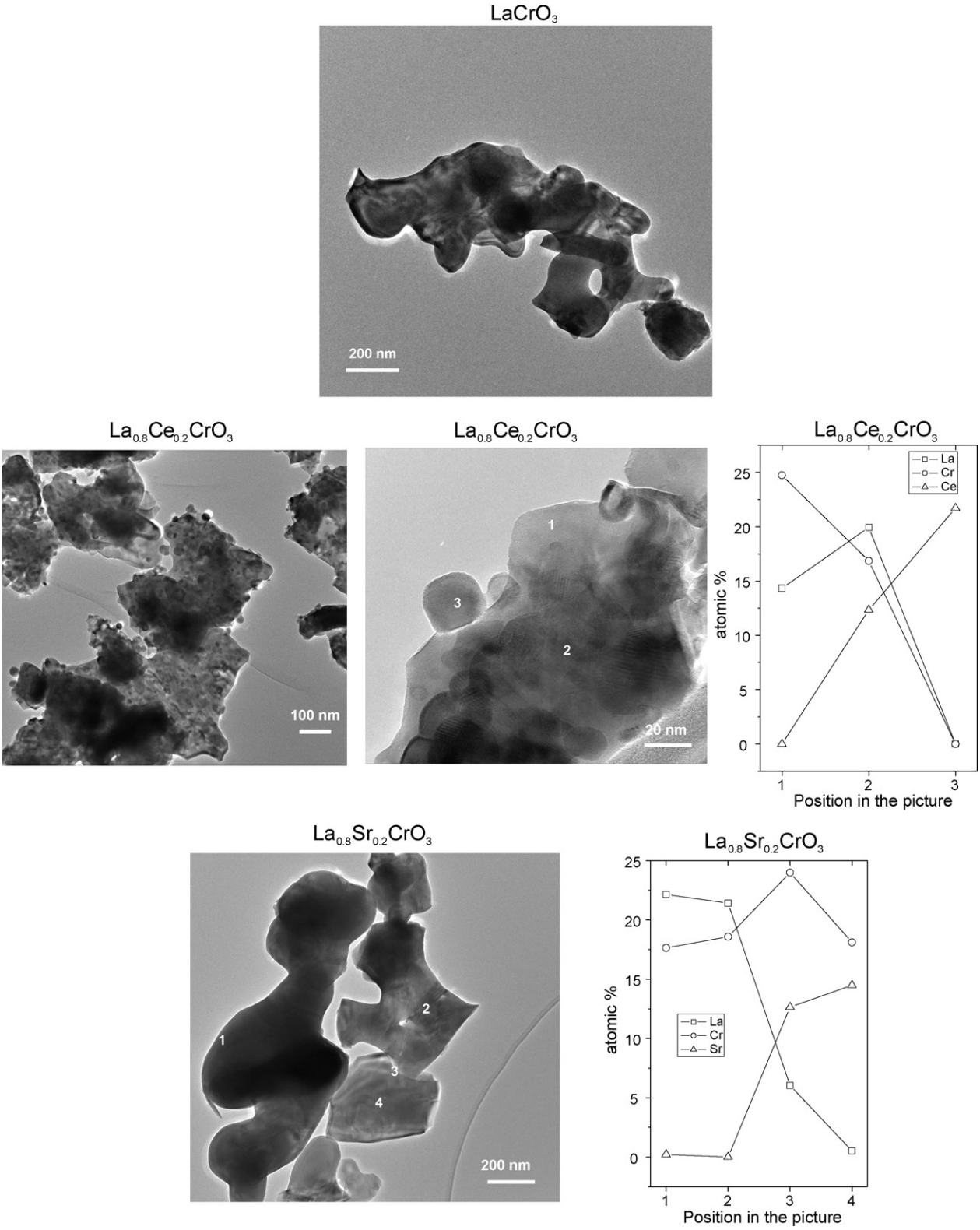

Fig. 6. Representative TEM images and XEDS analyses for the indicated samples.

amount of strontium into the chromite perovskite lattice of the doped samples, in an amount which appears higher for the $x = 0.2$ sample, is inferred from analysis of the EPR spectra. In the case of the Ce-doped samples, cerium appears essentially segregated (as well as chromium) in the form of separated oxide phases which form relatively small particles on top of $LaCrO_3$ particles.

The evolution of the specific surface area (decreasing with increasing the Sr content and the opposite for the Ce-doped samples, Table 1) is in agreement with previous investigations on materials of this kind [16,42–44]. Fig. 7 shows the SEM micrographs of the samples. Both large (>5 μm) and (predominantly) small (<1 μm) particles were generally observed in the

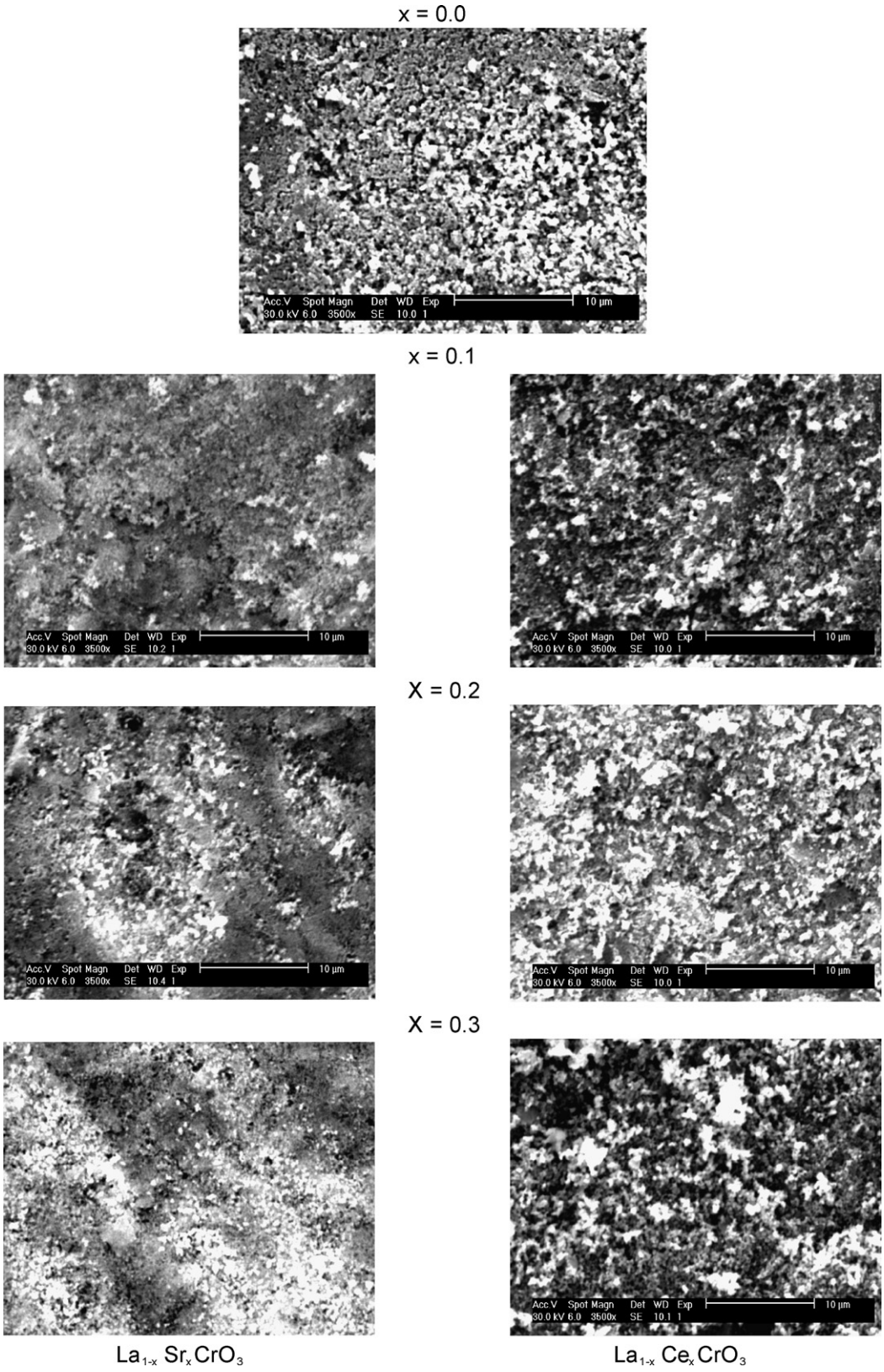

Fig. 7. SEM images of the $La_{1-x}M_xCrO_3$ (M = Sr or Ce; x = 0.0–0.3) samples.

pictures, in agreement also with TEM results, and must be related to aggregates of small crystallites. Average particles sizes for such aggregates are reported in Table 1 and appear in qualitative agreement with the evolutions observed in the S_{BET} values.

3.3. XPS surface analysis

The surface characteristics of the series of perovskites prepared by sol–gel and calcined at 800 °C were studied by XPS. Table 2 lists

Table 2
Binding energies of main peaks of core electrons and atomic percentages extracted from the XPS spectra for the $La_{1-x}M_xCrO_3$ (M = Sr or Ce) samples calcined at 800 °C

Sample	XPS binding energies (eV) of main peaks (relative percentages in parentheses)				% of the C 1s peak at 288.9 eV	Atomic percentages			
	La $3d_{5/2}$	Cr $2p_{3/2}$	O 1s	Sr $3d_{5/2}$ or Ce $3d_{5/2}$		La	Cr	O	Sr or Ce
$LaCrO_3$	834.9 838.7	576.6 (54) 579.6 (46)	529.8 (43) 531.6 (57)		31.5	15.28	17.72	67.00	
$La_{0.9}Sr_{0.1}CrO_3$	834.9 838.6	576.7 (57) 578.0 (43)	529.8 (43) 531.6 (57)	134.1	19.6	13.78	18.15	64.90	3.18
$La_{0.8}Sr_{0.2}CrO_3$	834.8 838.5	576.5 (58) 580.0 (42)	529.9 (63) 531.9 (37)	134.0	15.1	12.39	17.20	65.72	4.69
$La_{0.7}Sr_{0.3}CrO_3$	834.5 838.2	576.3 (56) 579.8 (44)	529.7 (60) 531.7 (40)	133.9	12.2	12.59	17.98	63.91	5.52
$La_{0.9}Ce_{0.1}CrO_3$	835.0 838.4	576.8 (58) 579.6 (42)	530.2 (66) 532.2 (34)	882.7	29.8	13.77	16.01	66.78	3.44
$La_{0.8}Ce_{0.2}CrO_3$	834.6 838.4	576.4 (61) 579.0 (39)	529.7 (63) 531.6 (36)	882.5	54.3	12.53	15.72	66.60	5.17
$La_{0.7}Sr_{0.3}CrO_3$	834.7 838.5	576.6 (64) 579.4 (36)	529.8 (65) 531.7 (35)	882.6	34.5	11.98	13.74	67.11	7.16

the binding energies of most representative peaks of the La 3d, Sr 2p, Ce 2p, Cr 2p and O 1s levels, as well as atomic percentages of these elements determined from the spectra after employment of appropriate experimental sensitivity factors [23]. Fitted XPS spectra of most relevant regions of the two sample series are displayed in Fig. 8.

No significant differences between the samples were detected in the La 3d zone (spectra not shown), which displayed the typical double peak profile of La $3d_{3/2}$ components located at ca. 855.3 and 851.2 eV while the typical two peaks of La $3d_{5/2}$ components appeared at ca. 838.5 and 834.7 eV, respectively (Table 2). These are close to the values recorded for lanthanum within oxidic environments [45]. For the O 1s zone, the spectra are in all cases consistent with the presence of two peaks (Table 2): a low binding energy one at ca. 529.9 eV, which is typically attributed to lattice oxide species, and a peak at ca. 531.7 eV, which is assigned to surface adsorbed oxygen species typically in the form of carbonate or hydroxyl species [46]. In this sense, analysis of the C 1s region, in

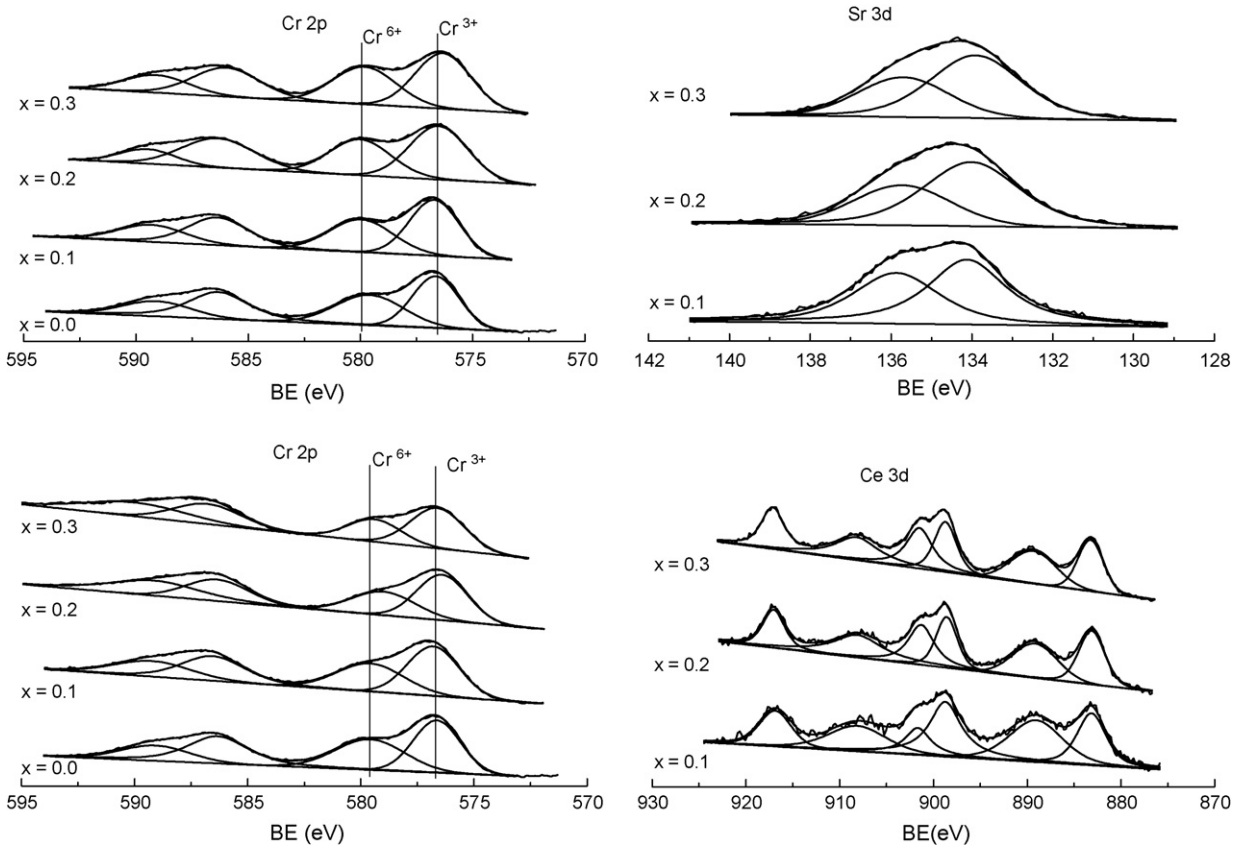

Fig. 8. Core level XPS spectra of most relevant spectral zones. Top: $La_{1-x}Sr_xCrO_3$ samples. Bottom: $La_{1-x}Ce_xCrO_3$ samples.

which in addition to the spurious peak at 284.6 eV (see Section 2), a peak at 288.9 eV is detected which could be attributed to carbonate species (Table 1), indicates a predominance of hydroxyl species as main contribution to the surface oxygen signal in the Sr-doped series while a more important contribution of carbonates to such signal is inferred for the samples of the Ce-doped series.

The Cr 2p spectra display peaks characteristic of the presence of at least two distinct valence states of chromium, with two Cr $2p_{3/2}$ components at ca. 576.5 and 579.5 (Fig. 8 and Table 2). According to results in the literature for pure oxides, the two mentioned peaks can most likely be related to the presence of Cr^{3+} (or Cr^{4+}, showing relatively small shift with respect to Cr^{3+}) and Cr^{6+}, respectively [18,47,48]. Noteworthy, no significant differences are detected in the intensity ratio between both components as a function of the degree of doping. This contrasts, at least in the case of Sr-doped samples, with results observed for samples prepared by solid state reaction in which a higher contribution of the Cr^{6+} component was detected for $x = 0.3$ [18]. This can nevertheless be masked by the presence of a certain amount of Cr^{6+} even for the non-doped $LaCrO_3$ specimen, which is a usual feature in this kind of chromium perovskite samples [49]. Nevertheless, the fact that strontium chromate apparently forms well separated particles (instead of segregating on top of the lanthanum chromite particles) as well as the fact that Cr^{3+} can be most favoured in the presence of surface oxyhydroxide-type complexes (in accordance to the relatively large component of entities related to adsorbed species in the O 1s zone) could balance the contribution expected from the presence of chromate species [29].

The XPS results of the Ce 3d core level of the $La_{1-x}Ce_xCrO_3$ samples (Fig. 8) are similar to those detected for fully oxidised cerium oxide (CeO_2) [50,51], thus revealing that most of the cerium appears in a Ce^{4+} chemical state and none or very little Ce^{3+} must be present. This is also consistent with the intensity detected for the Ce $3d_{3/2}$ peak around 916.3 eV with respect to that of the second "shake-up" satellite of Ce $3d_{5/2}$ (signal centred at 882.1–882.3 eV), and whose ratio of ca. 1.5 is consistent with a predominance of Ce^{4+} in all the samples. Concerning the Sr 3d zone, the results are consistent with the presence of a single signal (separated in the corresponding Sr $3d_{5/2}$ and $2d_{3/2}$) at a binding energy typical for Sr^{2+} into oxidic environments [52]. Nevertheless, it must be noted that no important differences would be expected for the Sr 3d spectra of two different oxidic phases like $SrCrO_4$ and $La_{1-x}Sr_xCrO_3$ [18].

Particular attention is paid to the evolution of the elemental contributions to the spectra as a function of the degree of doping and, in particular, to the Cr one which can be most relevant to the catalytic properties of this type of systems [1,18]. As displayed in Fig. 9, the relative chromium and strontium amounts detected by XPS for the catalysts of the $La_{1-x}Sr_xCrO_3$ series appear slightly higher than the nominal values for the whole series except for the $x = 0.3$ sample. An appreciable difference between the catalysts of this series and those of the $La_{1-x}Ce_xCrO_3$ one concerns the evolution of the Cr intensity (Fig. 9 and Table 2), which is appreciably lower in the catalysts of the latter series, particularly for doping levels $x > 0.1$ for which it even lies below expected nominal levels. In contrast, the amount of cerium detected indicates a cerium enrichment in all cases which suggests that the cerium oxide entities detected by XRD must basically locate at the surface of the samples, in agreement with TEM–XEDS results (Fig. 6) and with previous exploration by electron microscopy of other samples of this type [43].

3.4. Catalytic activity for C_3H_6 combustion

The catalytic activities of the lanthanum chromite for C_3H_6 combustion (no other products than those of full oxidation were detected in the infrared gas analyser) were apparently modified upon doping with Sr and Ce. Appreciable differences were detected as a function of the dopant nature and its respective amount, as collected by Figs. 10 and 11. Another general aspect concerns the higher activity of the Sr-doped samples with respect to those of the Ce-doped catalysts, as more clearly revealed upon comparison of the specific activities, displayed in Fig. 11.

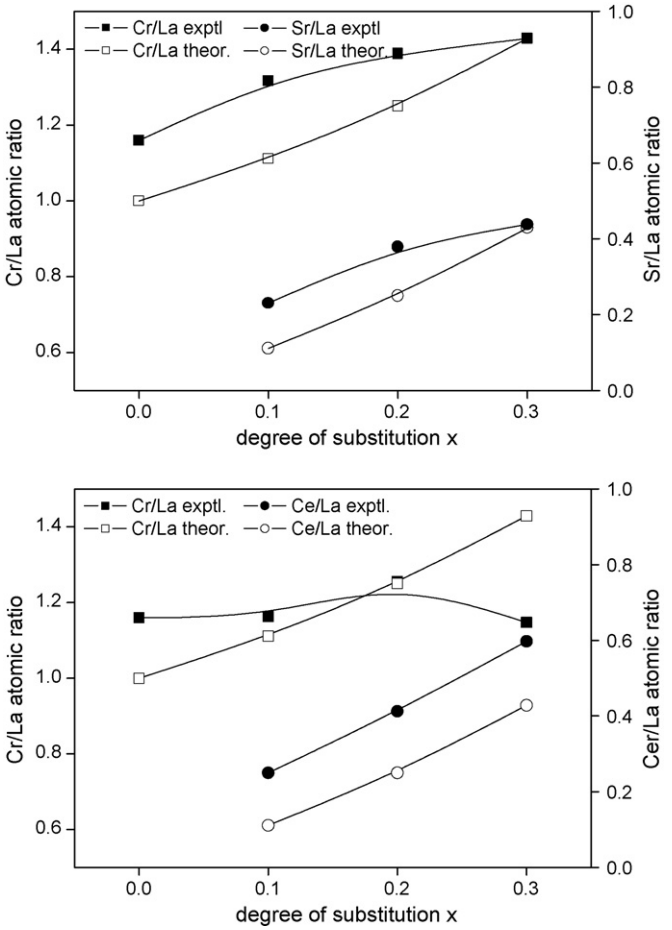

Fig. 9. Evolution of the indicated atomic ratios detected by XPS as a function of the doping degree x (full symbols). Corresponding nominal values are displayed as open symbols.

In the case of Sr-doped samples, a maximum activity is detected for $x = 0.2$ while a small gradual increase is observed with increasing the cerium content of the Ce-doped series, as a consequence of the specific area increase induced by such doping (Figs. 10 and 11 and Table 1). Nevertheless, analysis of the specific activities in this latter indicates only a slight activity enhancement for the $x = 0.1$ system while apparent activity decrease is observed for higher doping level. This indicates a general detrimental effect of the presence of ceria and its surface segregation to the sample surface leading to decreases in the surface chromium content at the surface in agreement with XPS results (Fig. 9). Indeed, independent experiments with a pure CeO_2 catalyst showed an appreciably lower C_3H_6 conversion level (not shown) than for any of the $La_{1-x}Ce_xCrO_3$ samples, thus supporting a negligible contribution of such segregated CeO_2 particles to the overall activity.

Results in the literature show that Sr or Ce substitution for La in slightly doped $LaMO_3$-type perovskites generally improves the hydrocarbon oxidation catalytic activity [1,53,54]. This is generally explained on the basis of introduction of defects, like oxygen

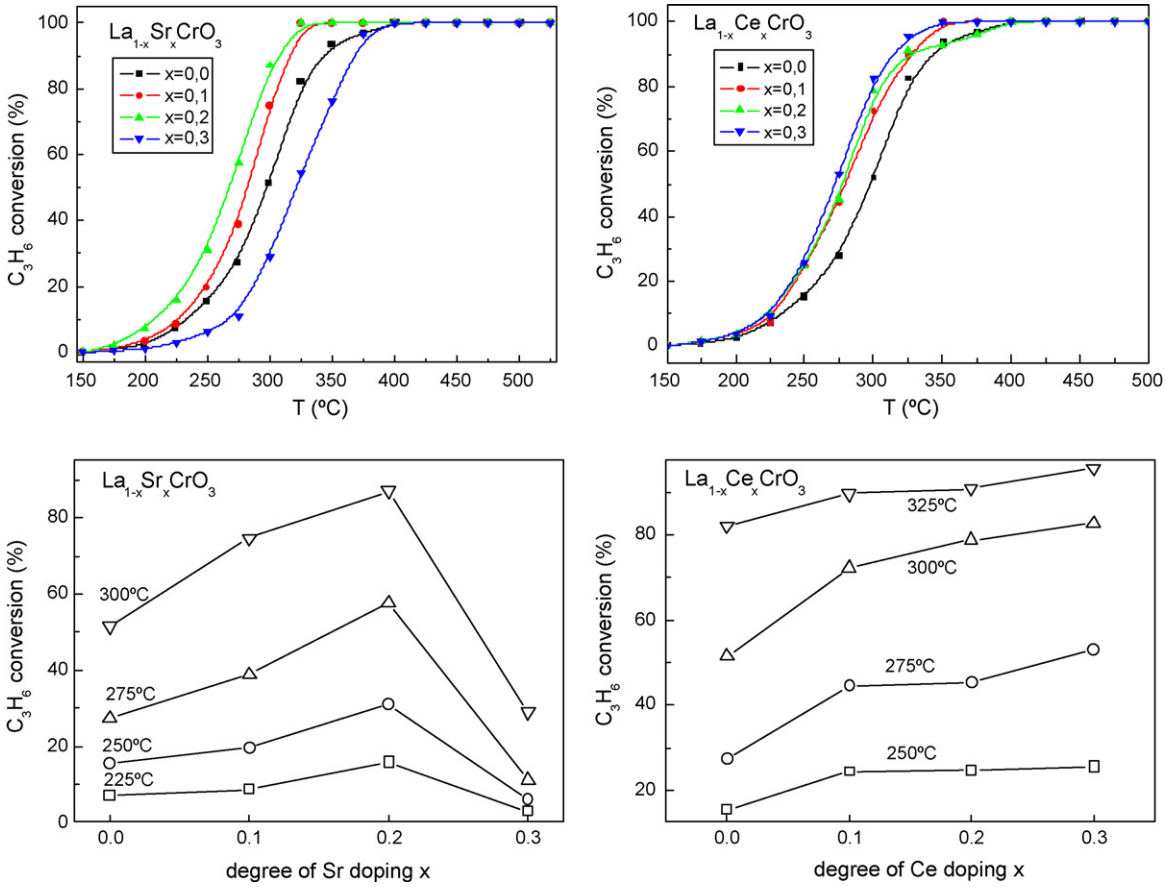

Fig. 10. Results of catalytic activity for C_3H_6 combustion reactions over the catalysts of the $La_{1-x}Sr_xCrO_3$ (left) and $La_{1-x}Ce_xCrO_3$ (right) series.

vacancies, or changes in the chromium valence state (from Cr^{3+} to Cr^{4+}) following substitution of A-site in ABO_3. Such modifications could enhance oxygen transport or redox activity of the chromium surface centers thus enhancing hydrocarbon oxidation properties known to be affected by such properties within a suprafacial mechanism of application to our case [1,54,55]. Other factors like the amount of surface chromium, considered as most active component, as a function of doping level (Fig. 9), or effects of cooperation between different segregated oxide phases could also be relevant to the oxidation catalysis [1,56]. Nevertheless, it must be noted that direct correlation between activity results and XPS surface characteristics of the samples cannot be established as a consequence of difficulties to separate Cr^{3+} and Cr^{4+} contributions and considering also the uncertainty of surface contributions to the former from possible oxyhydroxyde species present. In any case, the results indicate that the propylene oxidation activity is enhanced upon doping of the lanthanum chromite by Sr (even if at a relatively weak level, according to characterization results mainly by XRD and EPR), in agreement with previous findings on samples prepared by solid state reaction [18], as well as with earlier literature results [1,54]. However, in general terms, segregation of dopants and part of the chromium in oxide phases upon doping and formation of multiphase systems do not appear to affect appreciably the oxidation activity of this type of chromite perovskites, in contrast to observations for cerium-doped cobaltite perovskites [56].

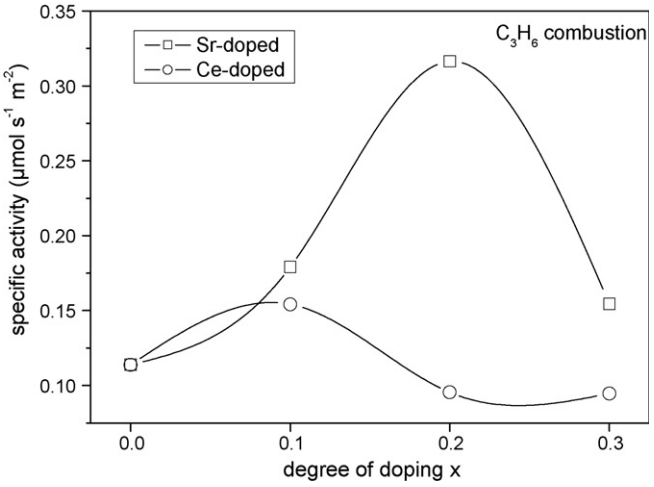

Fig. 11. Specific (surface area normalized) activities of the indicated samples for C_3H_6 combustion at 275 °C.

4. Conclusions

Two series of $La_{1-x}M_xCrO_3$ ($x = 0.0$, 0.1, 0.2 and 0.3) catalysts doped with M = Sr and Ce, respectively, have been prepared by sol–gel. TG/TDA analysis of the solid precursors after treatment in an oven at 80 °C evidences that full decomposition of the organic molecules or intermediate oxides and generation of the lanthanum chromite perovskite phase (according also to XRD examination) is produced for $T >$ ca. 800 °C. XRD analysis of the samples calcined at 800 °C reveal the presence of a major lanthanum chromite perovskite phase in all cases although significant degree of segregation of the dopant is also detected. It apparently forms

monazite $SrCrO_4$ in the Sr-doped samples while CeO_2 and Cr_2O_3 phases appear in the Ce-doped samples. Nevertheless, EPR analysis allows to conclude on partial introduction of Sr (maximum for $x = 0.2$) into the lanthanum chromite perovskite phase. The presence of such segregated phases is also confirmed by TEM–XEDS. The catalytic activity for C_3H_6 combustion is observed to increase with the doping level for the Ce-doped samples although this appears only a consequence of concomitant specific area increases. In contrast, maximum specific activity is observed for $x = 0.2$ in the Sr-doped samples which evidences the beneficial catalytic effect of Sr introduction into the lanthanum chromite structure.

Acknowledgements

K. R thanks the Ministere de l'Enseignement Superieur et de la Recherche Scientifique of Algeria for a grant under which part of this work was performed. Thanks are due to the ICP-CSIC Unidad de Apoyo staff and Mr. E. Pardo for performing the adsorption isotherms and XPS spectra, respectively, as well as to Dr. Laura Pascual for performing the TEM–XEDS experiments. Financial support by Comunidad de Madrid (ENERCAM project ref. S-0505/ENE/000304) and MEC-Plan Nacional (CTQ2006-15600/BQU) is acknowledged.

References

[1] M.A. Peña, J.L.G. Fierro, Chem. Rev. 101 (20011981) (and references therein).
[2] H. Taguchi, S.-I. Matsuura, M. Nagao, H. Kido, Phys. B 270 (1999) 325.
[3] F. Boroomand, E. Wessel, H. Bausinger, K. Hippert, Solid State Ionics 129 (2000) 251.
[4] R.T. Baker, I.S. Metcalfe, Appl. Catal. A 126 (1995) 297.
[5] G. Saracco, G. Scibilia, A. Iannibello, G. Baldi, Appl. Catal. B 8 (1996) 229.
[6] M-F.M. Zwinkels, O. Hanssner, P.-G. Menon, S.-G. Jaras, Catal. Today 47 (1999) 73.
[7] K. Huang, J. Wan, J.B. Goodenough, J. Mater. Sci. 36 (2001) 1093.
[8] A.-L. Sauvet, J. Fouletier, J. Power Sources 101 (2001) 259.
[9] J. Sfeir, P.A. Buffet, P. Möckli, N. Xanthopoulos, R. Vasquez, H.J. Mathieu, J. van Herle, K.R. Thampi, J. Catal. 202 (2001) 229.
[10] P. Vernoux, E. Djurado, M. Guillodo, J. Am. Ceram. Soc. 10 (2001) 2289.
[11] J.W. Fergus, Solid State Ionics 171 (2004) 1.
[12] S.P. Jiang, J.P. Zhang, X.G. Zheng, J. Eur. Ceram. Soc. 22 (2002) 361.
[13] K. Hilpert, R.W. Steinbrech, F. Borromand, E. Wessel, F. Meschke, A. Zuev, O. Teller, H. Nikel, J. Eur. Ceram. Soc. 23 (2003) 3009.
[14] S.J. Kim, G.R. Demazeau, I.G. Presniakov, J.H. Choy, J. Solid State Chem. 161 (2001) 197.
[15] F.-C. Buciuman, F. Patcs, J.C. Menezo, J. Barbier, T. Hahn, H.-G. Lintz, Appl. Catal. B 35 (2002) 175.
[16] M. Alifanti, J. Kirchnerova, B. Delmon, Appl. Catal. A 245 (2003) 231.
[17] K.S. Song, H. Xing-Cui, S.-D. Kim, S.-K. Kang, Catal. Today 47 (1999) 155.
[18] K. Rida, A. Benabbas, F. Bouremmad, M.A. Peña, A. Martinez-Arias, Catal. Commun. 7 (2006) 963.
[19] A.A. Leontiou, A.K. Ladavos, T.V. Bakas, T.C. Vaimakis, P.J. Pomonis, Appl. Catal. A 241 (2003) 143.
[20] M.R. Goldwasser, M.E. Rivas, E. Pietri, M.J. Perez-Zurita, M.L. Cubeiro, L. Gingembre, L. Leclercq, G. Leclercq, Appl. Catal. A 255 (2003) 45.
[21] G.K. Williamson, W.H. Hall, Acta Metall. 1 (1953) 22.
[22] A. Weibel, R. Bouchet, F. Boulch, P. Knauth, Chem. Mater. 17 (2005) 2378.
[23] C.D. Wagner, L.E. Davis, M.V. Zeller, J.A. Taylor, R.H. Raymond, L.H. Gale, Surf. Interface Anal. 3 (1981) 211.
[24] P. Durán, J. Tartaj, F. Capel, C. Moure, J. Eur. Ceram. Soc. 24 (2004) 2619.
[25] S. Bilger, G. Blab, R. Förthman, J. Eur. Ceram. Soc. 17 (1997) 1027.
[26] S. Biamino, C. Badini, J. Eur. Ceram. Soc. 24 (2004) 3021.
[27] P.S. Debi, M.S. Rao, J. Anal. Appl. Pyrolysis 22 (1992) 187.
[28] A.C. Tas, P.J. Majewski, F. Aldinger, J. Am. Ceram. Soc. 83 (2000) 2954.
[29] K. Rida, A. Benabbas, F. Bouremmad, M.A. Peña, E. Sastre, A. Martinez-Arias, Appl. Catal. A 327 (2007) 173.
[30] J.D. Carter, H.U. Anderson, M.G. Shumsky, J. Mater. Chem. 31 (1996) 551.
[31] Catalysis by Ceria and Related Materials. A. Trovarelli (ed), Imperial College Press, 2002.
[32] C.P. Khattak, D.E. Cox, Mater. Res. Bull. 12 (1977) 463.
[33] K. Tezuka, Y. Hinatsu, A. Nakamura, T. Inami, Y. Shimojo, Y. Morii, J. Solid State Chem. 141 (1998) 404.
[34] P.S. Debi, M.S. Rao, J. Solid State Chem. 98 (1992) 237.
[35] S. Miyoshi, S. Onuma, A. Kaimai, H. Matsumoto, K. Yashiro, T. Kawada, J. Mizusaki, H. Yokokawa, J. Solid State Chem. 177 (2004) 4112.
[36] M. Fernández-García, A. Martínez-Arias, J.C. Hanson, J.A. Rodríguez, Chem. Rev. 104 (2004) 4063.
[37] D. Cordischi, S. De Rossi, M. Faticanti, G. Minelli, P. Porta, Phys. Chem. Chem. Phys. 4 (2002) 3085.
[38] H. Effenberger, F. Pertlik, Z. Kristallogr. 176 (1986) 75.
[39] R. Ganguly, I.K. Gopalakrishnan, J.V. Yakhmi, J. Phys. Condens. Matter. 12 (2000) L719.
[40] S.A. French, C.R.A. Catlow, R.J. Oldman, S.C. Rogers, S.A. Axon, Chem. Commun. (2002) 2706.
[41] M. Cherian, M.S. Rao, A.M. Hirt, I.E. Wachs, G. Deo, J. Catal. 211 (2002) 482.
[42] K.S. Chan, J. Ma, S. Jaenicke, G.K. Chuah, J.Y. Lee, Appl. Catal. A 107 (1994) 201.
[43] Y. Zhang-Steenwinkel, J. Beckers, A. Bliek, Appl. Catal. A 235 (2002) 79.
[44] T. Kuznetsova, V. Sadykov, L. Batuev, E. Moroz, E. Burgina, V. Rogov, L. Kurina, S. Neophytides, React. Kinet. Catal. Lett. 86 (2005) 249.
[45] Y. Uwamino, T. Ishizuka, H. Yamatera, J. Electron Spectrosc. Rel. Phenom. 34 (1984) 67.
[46] S. Ponce, M.A. Peña, J.L.G. Fierro, Appl. Catal. B 24 (2000) 193.
[47] R. Merryfield, M. McDaniel, G. Parks, J. Catal. 77 (1982) 348.
[48] B. Wichterlova, L. Krajcikova, Z. Tvaruskova, S. Beran, J. Chem. Soc. Faraday Trans. 80 (1984) 2639.
[49] N. Russo, D. Fino, G. Saracco, V. Specchia, J. Catal. 229 (2005) 459.
[50] J.P. Holgado, R. Alvarez, G. Munuera, Appl. Surf. Sci. 161 (2000) 301.
[51] A. Martínez-Arias, M. Fernández-García, A.B. Hungría, J.C. Conesa, G. Munuera, J. Phys. Chem. B 107 (2003) 2667.
[52] M.I. Sosulnikov, Y.A. Teterin, J. Electron Spectrosc. Rel. Phenom. 59 (1992) 111.
[53] T. Nitadori, S. Kurihara, M. Misono, J. Catal. 98 (1986) 221.
[54] N. Yamazoe, Y. Teraoka, Catal. Today 8 (1990) 175 (and references therein).
[55] R.J.H. Voorhoeve, J.P. Remeika, L.E. Trimble, Ann. N. Y. Acad. Sci. 272 (1976) 3.
[56] J. Kirchnerova, M. Alifanti, B. Delmon, Appl. Catal. A 231 (2002) 65.